INVESTIGATION OF THE TRAUMATIC RUPTURE OF THE AORTA (TRA) BY SIMULATING REAL-WORLD ACCIDENTS

Chirag S. Shah, Warren N. Hardy, King H. Yang
Bioengineering Center, Wayne State University, Detroit, MI, USA

Chris A. Van Ee
Design Research Engineering, Novi, MI, USA

Richard M. Morgan and Kennerly H. Digges
The George Washington University, Ashburn, VA, USA

ABSTRACT

Traumatic rupture of the aorta (TRA) is one of the causes of death in automotive crashes. The risk of fatality is higher if the injury is not detected and treated promptly. Numerous laboratory experiments, retrospective studies, and theories with focus on TRA have yielded limited success.

Four real-world accidents with aortic injuries to the occupants were simulated using finite element (FE) methods. Two crashes were side impact, and the other two were frontal crashes. A two-phase approach was used. For Phase 1, car-to-car interaction was simulated using vehicle FE models. These simulations were validated qualitatively and quantitatively against available crash photographs and crush data. For Phase 2, interaction between the occupant and the interior of the automobile was simulated using input obtained as a result of the first phase simulation. The occupant was a mid-sized male whole-body human FE model developed at Wayne State University.

For the two side impact crashes, the peri-isthmic region demonstrated the greatest maximum principal strain (MPS) and longitudinal stress (LS). For the frontal crashes, the junction of the ascending aorta and the aortic arch was the region of greatest MPS and LS. Peak MPS and peak LS averaged within the peri-isthmic region of the aorta for the second phase FE simulations ranged from 0.072 to 0.160, and 0.93 MPa to 1.58 MPa, respectively.

These FE simulations demonstrate feasibility of the approach of using FE vehicles and FE occupant model to investigate the underlying mechanisms of the TRA. The results also have potential application to the design of experiments to study TRA in cadavers.

Keywords: aorta, trauma, finite element model, human body, accident reconstruction

TRAUMATIC RUPTURE OF THE AORTA (TRA) is said to be the second most common cause of death (Sauaia et al. 1995) associated with motor vehicle crashes (MVC). It is considered to be responsible for approximately 8,000 fatalities every year in the United States (Mattox 1989). Roughly seventy percent of all TRA result from high speed MVC (Burkhart et al. 2001). McGwin et al. (2003) found that TRA occurs predominantly in frontal and near-side impact, corresponding to 45% and 22.5% of the TRA cases respectively. Even though the overall occurrence of TRA was higher in frontal MVC, the rate of TRA in near-side MVC was found to be twice that in frontal MVC (Steps 2003). Katyal et al. (1997) found aortic tears confined to the peri-isthmic region of the aorta in ninety-four percent of all TRA. Also, the aortic tears were found nearly always transverse to the long axis of the vessel (Zehnder 1960). Strassman (1947) found the intima and media of the aorta typically involved in TRA.

Several theories for TRA injury mechanisms such as downward traction (Letterer 1924), deceleration (Zehnder 1960), intravascular pressure (Klotz and Simpson 1932), osseous pinch (Crass et al. 1990), "Voigt's Shoveling" (Voigt and Wilfert 1969), and "Water Hammer" (Lundevall 1964) have been postulated. Various laboratory experiments aimed at producing TRA have yielded limited success. Accordingly, the underlying mechanisms are not very well understood.

FE modeling is becoming an increasingly important tool for understanding the mechanisms of TRA. Shah et al. (2001) developed a FE model of the human thorax. Simulations of thoracic impacts

from a number of directions indicated that the ligamentum arteriosum, subclavian artery, parietal pleura, and pressure changes within the aorta are factors that can influence aortic rupture. The aortic isthmus was shown to be the most likely site of aortic rupture regardless of impact direction. This model was then integrated with the FE abdomen model (Lee and Yang 2001) and FE shoulder model (Iwamoto et al. 2000) to develop a whole-body human FE model (Shah et al. 2004). Shah et al. (2005a) furthered these modeling efforts by conducting car-to-car simulations and simulating contact of the integrated whole-body human FE model with selected intra-vehicular structures. Similarly, the current study was designed to investigate mechanisms of TRA using simulated real-world MVC involving aortic injuries.

METHODS

Four real-world aortic injury cases were obtained from the National Automotive Sampling System (NASS) database. Several criteria were imposed when selecting these cases. The criteria were subject gender (male), height (170-180 cm), and weight (68-82 kg). Crush deformation (< 70 cm) and Delta-V (< 55 km/hr) were limited to non-catastrophic deformation patterns. For the cases selected, injury to the aorta represented the most severe injury, based on AIS rating. Cases of partial or complete ejection and rollover were excluded. The four selected crashes were numerically reconstructed in two phases.

For Phase 1 of each simulation, the FE vehicle models were obtained from the National Crash Analysis Center (NCAC) public FE model archive. If the model for the case vehicle or principal other vehicle (POV) was not available in the archive, a model providing the closest dimensional representation was selected and scaled, and the mass adjusted by adding lumped mass at the center of gravity. The occupant masses were adjusted by adding mass to the nodes of the driver and/or passenger seats. Initially, the two case vehicle models were positioned as noted by the crash reconstruction data in NASS. This required rotation and translation of both vehicle models before the simulation was conducted. The heavier of the two vehicles (to maximize energy) was given the appropriate initial velocity. Structural deformation patterns obtained in the simulations were compared with the real crash data. The simulations were repeated, tuning the impact position of the POV model until a reasonable match was obtained for the case vehicle crush data. For the side impact case vehicles, the driver side structures including the front and rear doorframe, door armrest, and left B-pillar nodes, were grouped and their motions were recorded in separate binary interface files using the *INTERFACE_*option* feature available in LS-Dyna (LSTC, Livermore, CA). These interface files were used to generate impact in the Phase 2 simulations. For frontal simulations, the acceleration pulse obtained at driver's seat during phase one was used for Phase 2 simulation.

For Phase 2 of each simulation, a sub-model of the case vehicle was extracted from the original model for interaction with the integrated FE human model. The human model includes detailed descriptions of the main bony structures, organs, and soft tissues of the human shoulder, thorax and abdomen (Figure 1a). In the torso region (Figure 1b), the model includes the main organs and vessels. The aorta, vena cava, lungs, heart, spleen, liver, kidneys, pleura, intercostals muscles, shoulder ligaments, shoulder muscles, and their associated tendons are modeled using deformable elements. An airbag filled with gas at atmospheric conditions represents the peritoneum with its visceral reflection covering the liver, spleen, and kidneys. The organs are surrounded by the rib cage and spine, which are also modeled with deformable elements. For this study, the model was updated to include the pericardium, parietal pleura, and kinematic joints for the hip, knee, and ankle joints. The integrated human FE model was imported into the case vehicle sub-model and was positioned in a seated posture. This posture was estimated based on post-crash photographs of the interior structures and seat. Each combined model was then setup for Phase 2 simulation.

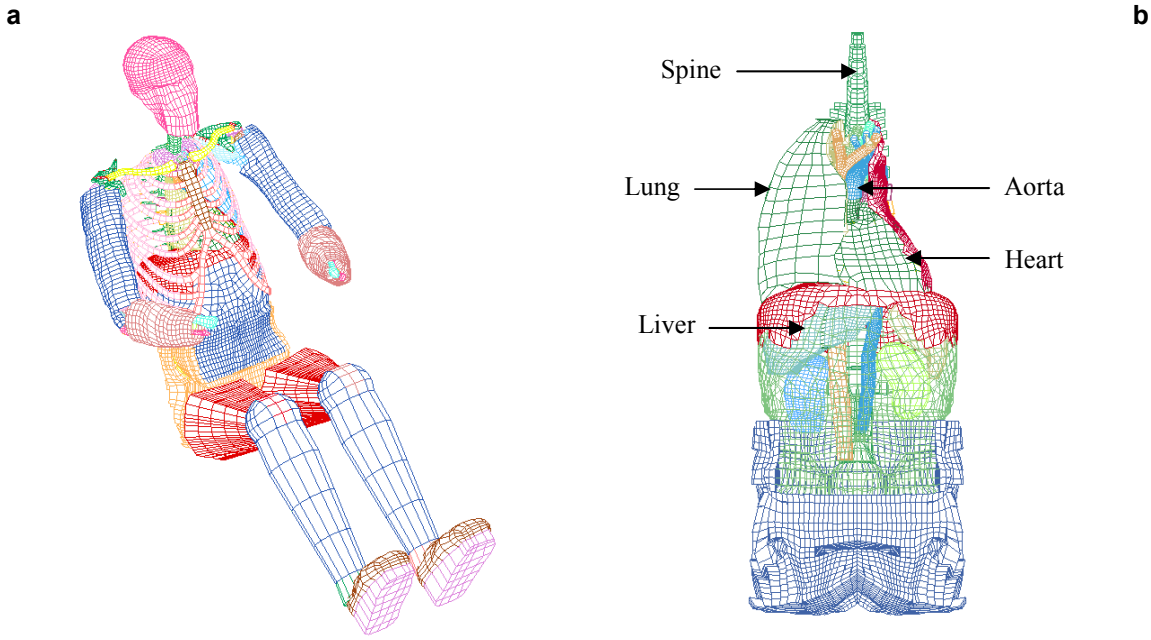

Figure 1 – The Overall Integrated Human FE Model (a), and Internal Organs (b)

CASE DESCRIPTION

Case #2000-79-149 : Vehicle one (V1) was disabled or parked facing southwest in the number three lane of a five-lane, dry, level, grooved concrete, physically divided roadway. Vehicle two (V2) was north bound in the same lane of the same roadway. The front of V2 impacted the left side of V1 and both cars came to rest in the number-four lane of the same roadway. Both cars were towed from the scene and the driver of V1 (male, 28, 180 cm, 68 kg) was hospitalized for a thoracic aorta laceration (AIS 5) and multiple injuries. The driver of V1 was not wearing any form of belt restraint, but the driver's frontal airbag deployed. Table 1 summarizes the actual crash vehicles and the representations used for the simulation. The mass is the value to which each FE vehicle was adjusted, and the scale factor is the value used to adjust the width and length of the FE vehicles. The Delta-V of the vehicle to which the initial speed was applied is also shown. Figure 2a shows the FE setup for the impact simulation.

Case #1997-11-207 : V1 was traveling north on a two lane rural roadway, approaching an intersection. V2 was traveling east on a two lane rural roadway, approaching the same intersection. The front of V2 contacted the left side of V1 in the intersection. The driver of V1 (male, 58, 155 cm, 68 kg) sustained AIS 4 injury to the thoracic aorta and multiple other injuries, and died. The driver of V1 was wearing a lap belt. The vehicle was not equipped with airbags. The driver of V2 was transported to the emergency room. Both vehicles were towed. Table 1 summarizes the actual crash vehicles and the representations used for the simulation. Figure 2b shows the FE setup for the impact simulation for this case.

Case #1997-82-214 : V1 was traveling in the number-1 lane of a 5-lane, two-way street. V2 was traveling in the opposite direction in the number-2 lane of the same road. V1 drifted left and contacted the left front of V2 with its left front. This caused V1 to rotate anticlockwise, and it contacted the front of a third vehicle in the number-3 lane with its right side. The driver of V1 was killed, and a front passenger of V1 sustained minor injuries, as did the driver of V2. The driver of V1 (male, 43, 175 cm, 71 kg) sustained 3 rib fractures and an incomplete laceration (AIS 4) of the thoracic aorta. The driver of V1 was not wearing a seatbelt, and the vehicle was not equipped with airbags. Table 1 summarizes the actual crash vehicles and the representations used for the simulation. Figure 2c shows the FE setup for the impact simulation for this case.

Case #1998-72-98 : V1 was traveling north on a two-lane road headed toward a "T" intersection. After stopping, V1 turned left onto the intersecting two-lane road. V2 was headed toward V1 on the intersecting road. The front of V1 hit V2 in the eastbound lane. The driver of V1 (male, 37, 175 cm, 73 kg) sustained a major laceration of the thoracic aorta (AIS 5) and was taken to the hospital. The driver and passenger of V2 were transported to the hospital as well. The driver of V1 was not wearing a seatbelt, and the vehicle was not equipped with airbags. Table 1 summarizes the actual crash vehicles and the representations used for the simulation. Figure 2d shows the FE setup for the impact simulation for this case.

Table 1. Summary of Actual and Simulated Vehicles

Case	Vehicle		Make and Model	Mass (kg)	Scale Factor	Delta-V (km/hr) Total, Longitudinal, Lateral
2000-79-149	1	actual	1996 Toyota Corolla	1052		
		simulated	Ford Taurus side impact		0.894	
	2	actual	1994 Ford Crown Victoria	1718		
		simulated	Dodge Neon		1.150	54, -41, 35
1997-11-207	1	actual	1992 Saturn SL	1057		
		simulated	Ford Taurus side impact		0.943	
	2	actual	1996 Plymouth Breeze	1331		
		simulated	Dodge Neon		1.060	43, -8, 42
1997-82-214	1	actual	1991 Toyota Cressida	1560		
		simulated	Honda Accord frontal impact		0.970	38, 38, 0
	2	actual	1995 Volvo 850	1516		
		simulated	Dodge Neon		1.000	
1998-72-98	1	actual	1989 GMC Sonoma	1371		
		simulated	Chevrolet S10 frontal impact		1.000	
	2	actual	1985 Chevrolet Astrovan	1767		
		simulated	Chevrolet C2500 frontal impact		1.200	46, 46, 0

RESULTS

Table 2 compares the measured crush values against those predicted during the first phase of FE simulation. The average difference between the actual vehicle deformations and the FE simulations ranged from -2 to -15 percent. Figure 3 shows the occupant interaction with the sub-modeled vehicle components at the time of maximal contact for all four cases. Time zero is specified as the initial contact between the vehicles. Figure 4 shows the resulting aorta deformation and the maximum principal strain pattern of the inner surface of the aorta for each of the FE simulations in anterior-posterior (AP) and lateral perspectives for the time of peak strain. The inner surface was examined because tears generally initiate on the inner surface, with the intima tearing first. Table 3 catalogs the average peak aorta response parameters that correspond to the patterns shown in Figure 4. The average peak longitudinal and circumferential true stress, peak Von-mises stress, maximum principal strain, and longitudinal and circumferential Lagrange strains are given as an average from four-to-six elements. The regions selected experienced the largest MPS within the peri-isthmic region that was

not associated with the insertion of the ligamentum arteriosum. Figure 5 provides the time histories for MPS, and longitudinal and circumferential Lagrange strain for all four FE cases of aortic injury. The relative time alignment between tests in this figure is arbitrary, and the curves extend to the point beyond which the simulations would not execute. The average longitudinal strains from the side impact simulations were considerably greater than the circumferential strains, and follow the time-history trends of the average maximum principal strains. The average circumferential strain from the frontal impact simulations are greater than the longitudinal strains, and follow the time-history trends of the average maximum principal strains.

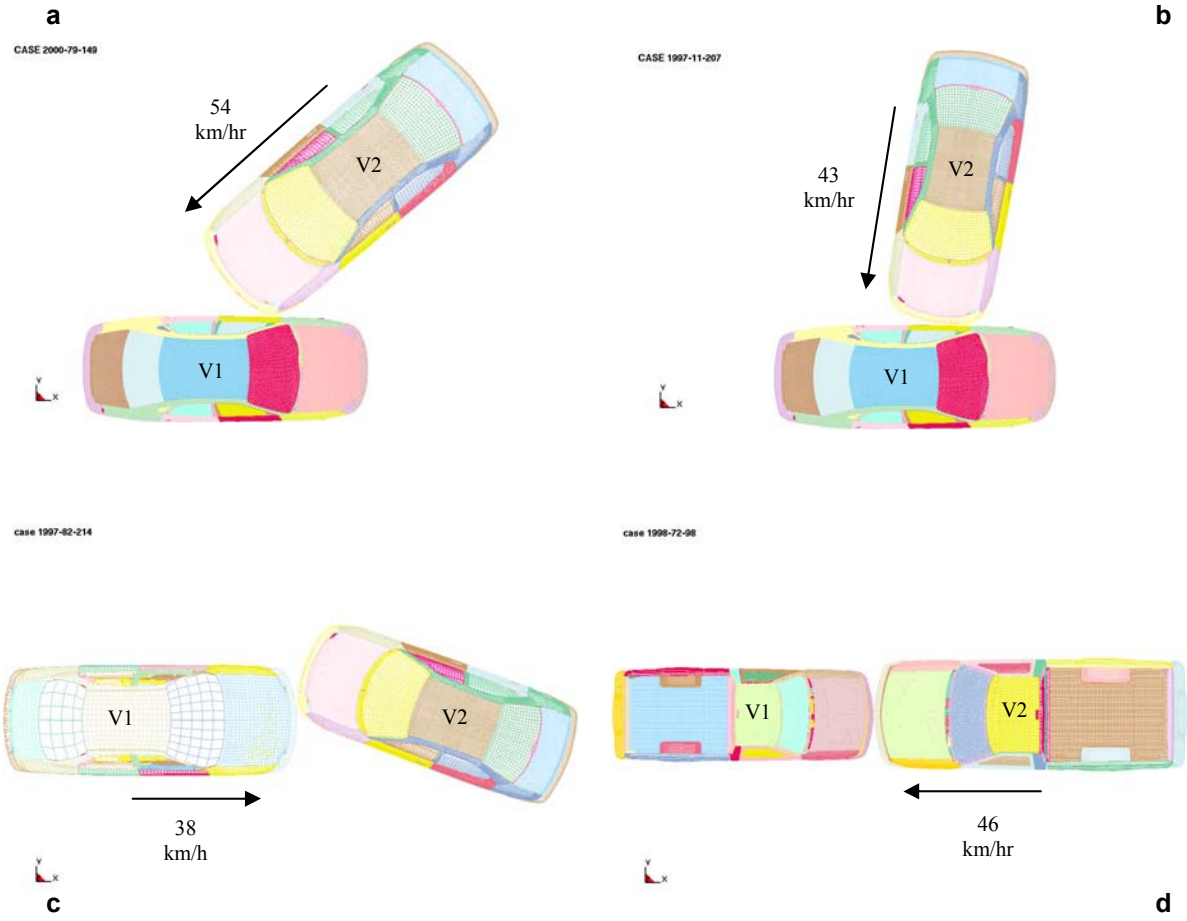

Figure 2 – The FE Impact Setup for Case #2000-79-149 (a), Case #1997-11-207 (b), Case #1997-82-214 (c), and Case #1998-72-98 (d)

Table 2. Comparison Between Actual and Finite Element Crush Values in mm

Case #	2000-79-149		1997-11-207		1997-82-214		1998-72-98	
Point	Actual	FE	Actual	FE	Actual	FE	Actual	FE
C1	0	*	160	*	650	571	690	580
C2	400	334	700†	380	670	546	590	520
C3	600	525	370	448	520	448	630	553
C4	300	265	450	382	310	352	660	574
C5	60	*	140	*	110	131	530	485
C6	0	*	0	*	0	0	580	493
Avg. Δ (%)		-9.7		-3.0		-2.4		-15.3

* Only C2-C4 (door deformation) were compared for the side impact cases.
† The rear door was removed for this measurement, making it artificially large (not used for Δ %).

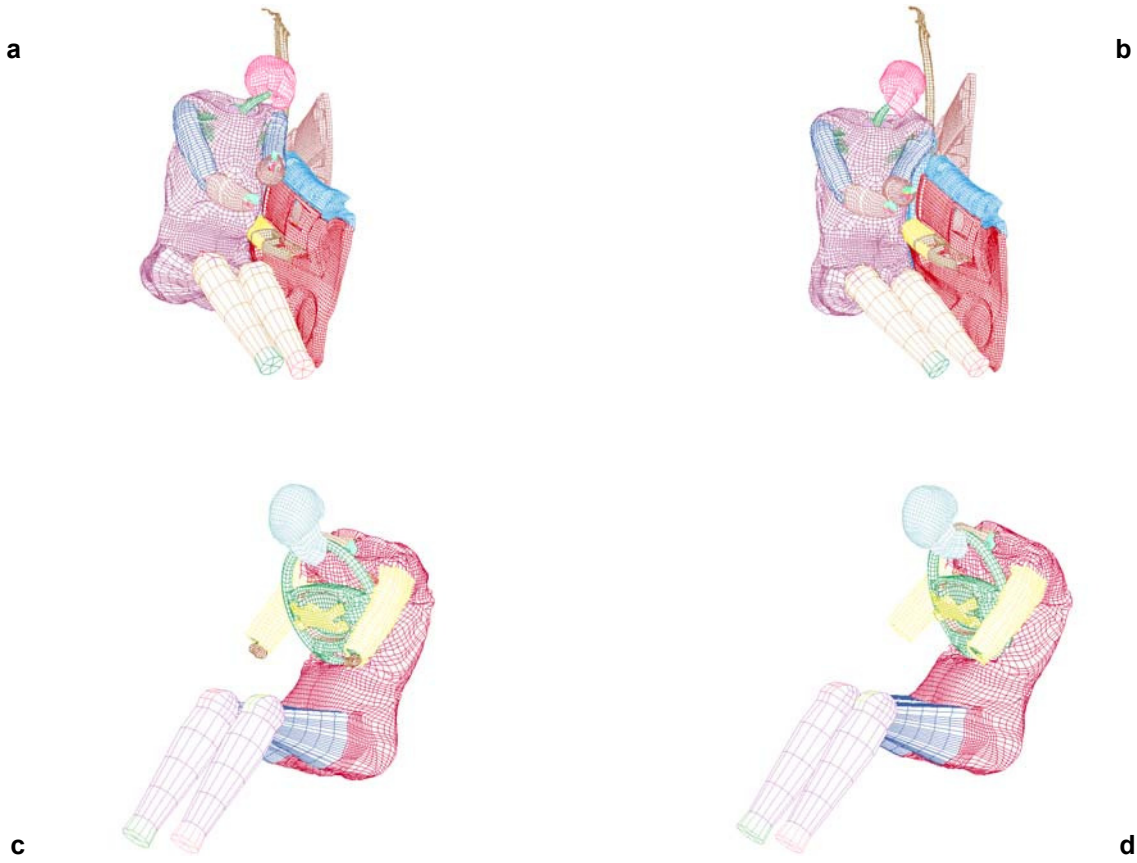

Figure 3 – The FE Occupant Interaction with the Sub-modeled Vehicle Components at the Time of Maximal Contact for Case #2000-79-149 (a), Case #1997-11-207 (b), Case #1997-82-214 (c), and Case #1998-72-98 (d)

Table 3. Peak Average Aorta Responses for the FE Simulations

Case #	Stress (MPa)			Strain		
	True		Von-mises	Maximum Principal	Lagrange	
	Longitudinal	Circumferential			Longitudinal	Circumferential
2000-79-149	1.28	0.51	1.68	0.160	0.123	0.032
1997-11-207	1.03	0.48	1.60	0.153	0.125	0.035
1997-82-214	0.93	0.93	0.97	0.072	0.059	0.062
1998-72-98	1.58	1.86	1.77	0.152	0.099	0.157
Avg.				0.134		

DISCUSSION

Four real world crashes with aortic injuries to occupants were simulated using FE techniques. These simulations demonstrated the feasibility of the approach of using FE vehicles and a FE occupant model to investigate the underlying mechanisms of TRA. No specific autopsy data were available in the NASS data regarding the locations of the aortic injuries for any of the cases. This shortcoming made direct comparison between the simulation and the real-world injury data impossible. Shah et al. (2005a) were able to make such direct comparison and found an excellent match between regions of

high strain in the model and actual injury data. However, the peri-isthmic region is known to be preferentially injured (Katyal et al. 1997) and to be relatively weak compared to other sections of the aorta (Lundevall 1964). Therefore, the simulation results are interpreted with respect to the peri-isthmic region, and the average stress and strain values were calculated for this region. The near side-impact cases exhibited the highest strain in the peri-isthmic region. The frontal impact cases resulted in the highest strain in the arch at the junction with the ascending aorta, followed by the peri-isthmic region. The insertion of the ligamentum arteriosum can create large strains at the point of insertion. However, since tears tend to initiate a distance from the insertion, the stress and strain values immediately at the insertion were not used for analysis. Compressive stresses and strain values were ignored in this study. The relatively high stress and strain demonstrated in the peri-isthmic region of the model suggests that the model response could be indicative of the actual injuries sustained in the crashes. Comparison to aorta failure thresholds is needed to provide a more complete understanding of the response and model limitations.

The FE simulations resulted in peak average longitudinal true stress ranging from 0.93 to 1.58 MPa (Table 3), which overlaps the lower end of the failure range shown in Table 4. The FE peak average maximum principal strain ranged from 0.072 to 0.160, which is roughly half the failure level derived from Shah et al. (2005b) on average. The longitudinal and circumferential Lagrange strains are also lower than the derived thresholds. As mentioned, the average longitudinal strains from the near side-impact simulations are considerably greater than the circumferential strains, and follow the time-history trends of the average maximum principal strains. The reverse is true for the frontal impact simulations, but the resulting average strains are still below threshold. These simulation results suggest that the peri-isthmic injury might be more closely associated to the strain.

The FE model demonstrates relative high strain at the junction of the ligamentum arteriosum and aorta for each simulation. This is considered to be a necessary artifact, and is assigned little importance because the ligament is not seen to separate from the aorta clinically, and sections of relative high stress and strain are seen throughout the peri-isthmic region. However, the ligamentum arteriosum representation seems to be related to abrupt shape changes in the arch (similar to a "kinked" garden hose) for some simulations. This kinked shape develops as the ascending aorta joins the arch as well.

There are a number of issues associated with the whole-body human FE model. It is validated against a variety of external inputs (Shah et al. 2001; 2004; 2005a). Still, these validations constitute a macroscopic level of validation only. The model used in this study benefited from the addition of the pericardium and parietal pleura, which are thought to be important to TRA injury mechanisms. However, there exists an artificial influence of the superior vasculature due to an abrupt termination and therefore tethering of the vessels at the neck. Further, there is no representation of the musculature beneath the manubrium that attaches to the viscera of the aortic arch. Similarly, there is no representation of the ligaments that tether the pericardium to the gladiolus. These structures are likely to be important to the mechanisms of TRA in side impact, in which anterior motion of the sternum due to rib deflection and force along the clavicles tends to pull the heart and arch away from the spine. However, the FE model contains a representation of the pericardium and central tendon, so motion of the heart is influenced by motion of the diaphragm, which may be important to TRA also.

Table 4. Aorta Failure Thresholds Derived from Shah et al. (2005b)

Test	True Stress (MPa)		Strain		
	Longitudinal	Circumferential	Maximum Principal	Lagrange	
				Longitudinal	Circumferential
A	1.39	1.72	0.265	0.252	0.170
B	1.59	1.89	0.346	0.258	0.289
C	2.31	2.47	0.301	0.232	0.205
D	1.31	1.54	0.280	0.186	0.257
E	2.05	1.60	0.414	0.334	0.347
Avg.	1.73	1.84	0.321	0.252	0.254

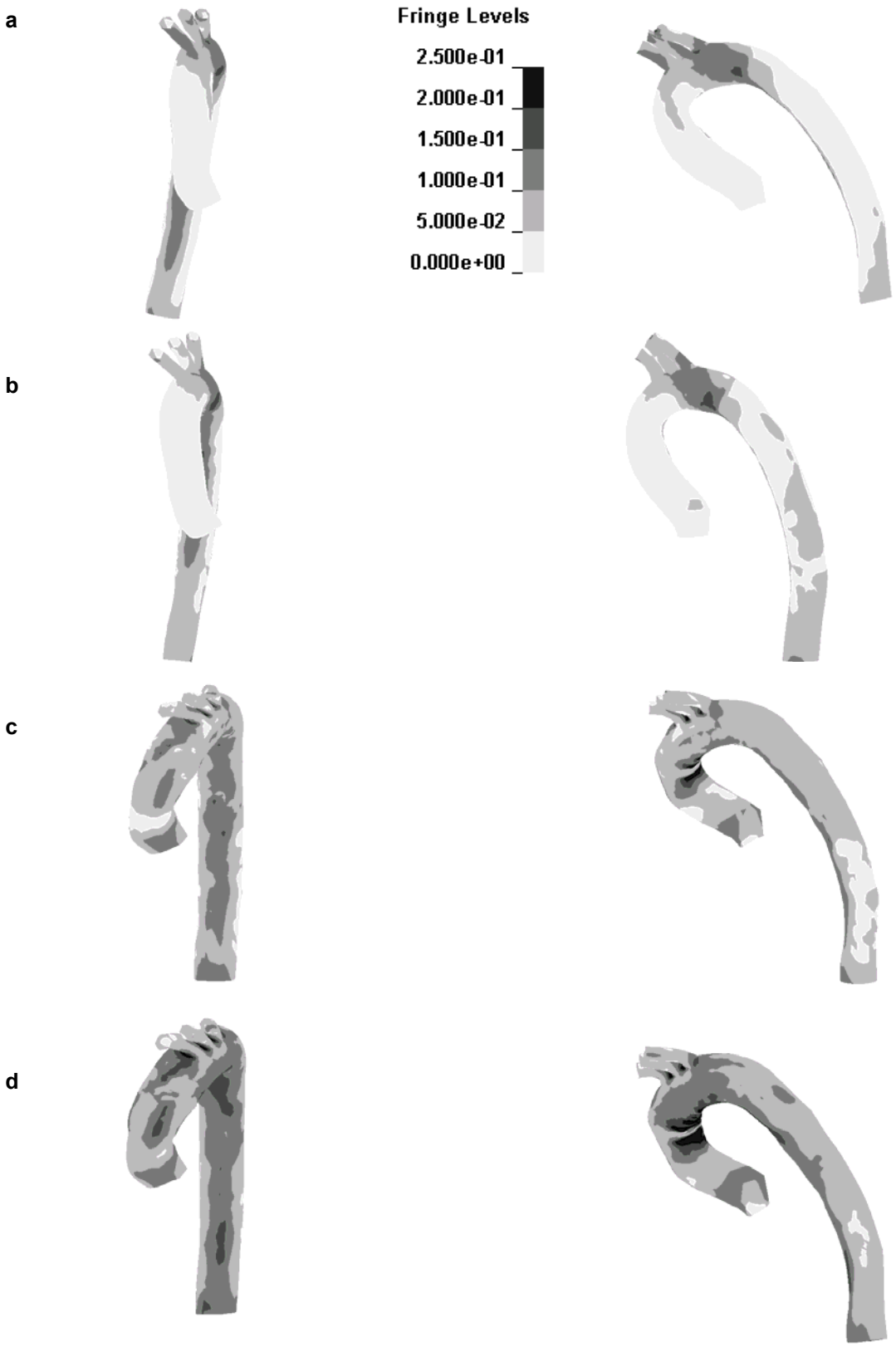

Figure 4 – AP (Left Column) and Lateral (Right Column) Perspectives of the Inner Surface Maximum Principal Strain Patterns for the FE Aortas Simulations from Case #2000-79-149 (a), Case #1997-11-207 (b), Case #1997-82-214 (c), And Case #1998-72-98 (d)

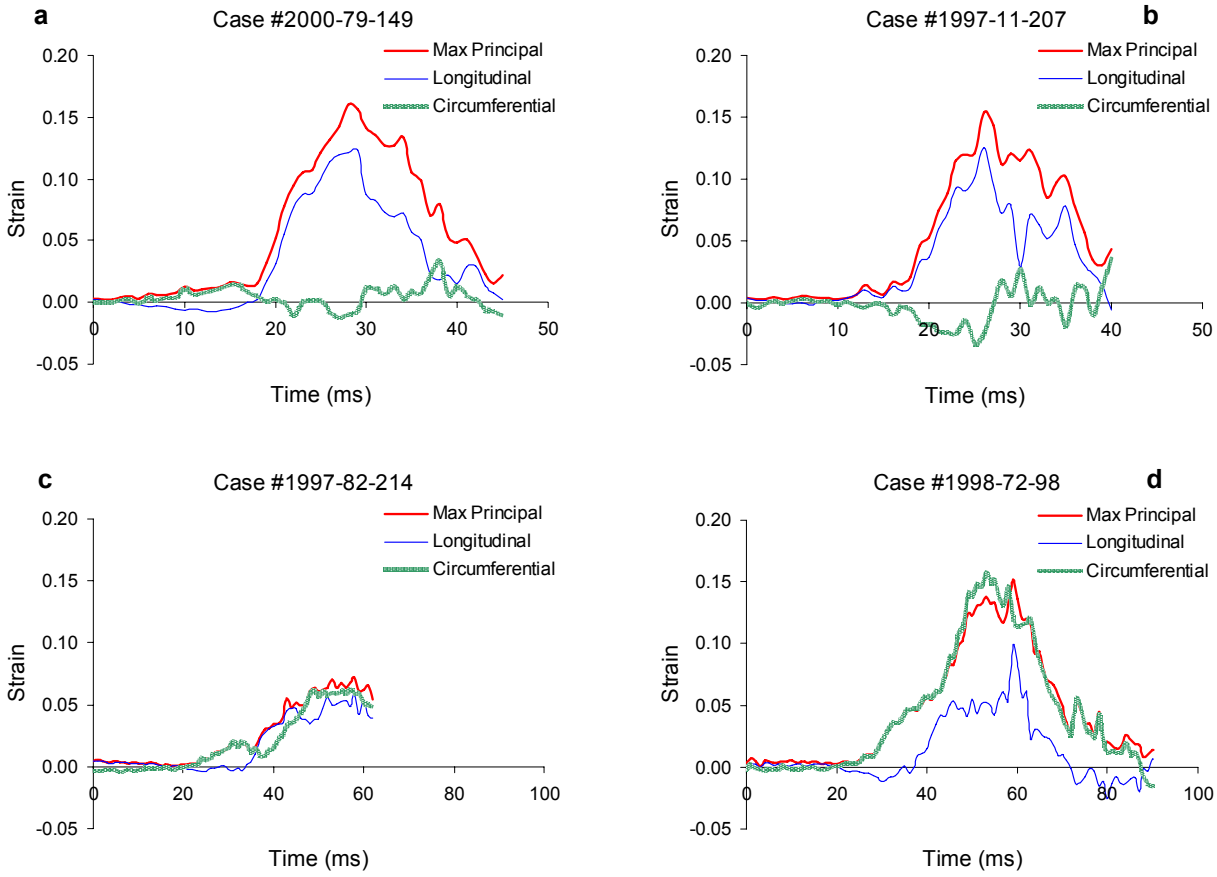

Figure 5 – Time-histories for the Average Maximum Principal, Longitudinal and Circumferential Lagrange Strain for the FE Aortas Simulations from Case #2000-79-149 (a), Case #1997-11-207 (b), Case #1997-82-214 (c), And Case #1998-72-98 (d)

A particular modeling challenge was the first phase of simulation: the car-to-car reconstructions. The exact models for the case vehicles were not always available in the NCAC library. Therefore, the closest approximating vehicles were selected and scaled. Another challenge for the frontal crash simulation was the front end representations of some of the vehicles. In some cases the structures were too stiff to produce the required crush values. In other cases structures were missing, requiring sections to be added to achieve the proper front end and bumper profiles. Although the average difference ranged from -2 to -15 % for all four cases (Table 2), individual differences in crush measurements were larger. The individual differences can be minimized only if more FE vehicle models are developed and made available at the NCAC. This will enable to simulate car-to-car simulations more closely. In general, attaining crush characteristics close to the measured deformation values was difficult and required multiple first-phase simulations to produce reasonably matching numbers.

Occupant position and posture influenced the Phase 2 simulations. Little data were available in the NASS database or any relevant reconstructions to help with locating and orienting the whole-body model within the vehicles. Estimates were obtained from combining accident investigation photographic records with subject anthropometry. The total effect of these estimates on occupant kinematics and interactions with interior structures of the vehicles is unknown, but is potentially substantial.

A final consideration is the constitutive properties for the FE representation of the aorta. In the current study, linear elastic material model with the Young's modulus of 10.0 MPa was assumed to represent the FE aorta. The value was taken from the dynamic biaxial experiments conducted on cruciate shaped aortic tissues from human cadavers (Shah et al. 2005b; 2006). The overall strain rate

for these tests was 102 sec^{-1}. Mohan (1976) conducted uniaxial tensile experiments on aortic strips from human cadavers at 100 sec^{-1} rate. The modulus in longitudinal direction was estimated in the range of 1.10 to 10.60 MPa. For the circumferential direction, the modulus ranged from 2.20 to 23.0 MPa. The modulus was estimated in the range of 6.70 to 31.00 for Mohan's (1976) biaxial bubble inflation tests at 20 sec^{-1} rate. These values were consistent with the experiments by Shah et al. (2005b; 2006). The low-strain, low-strain-rate, oscillatory tests of Bass et al. (2001) on porcine aortic tissues resulted in moduli an order of magnitude smaller. Development of a new material law is in progress based on new material properties determined by Shah et al. (2005b; 2006) and the aortic tissue modeling efforts reported by Maddali et al. (2005).

CONCLUSIONS

Traumatic rupture of the aorta has been studied using finite element simulations. A two-stage finite element approach has been implemented for the simulation of reconstructed, real-world, car-to-car collisions. It can be concluded that:

- finite element simulations demonstrate regions of relative high stress and strain in the peri-isthmic region for near side-impact cases, which is indicative of that seen clinically,
- finite element simulations demonstrate regions of relative high stress and strain in the peri-isthmic region and the junction of the ascending aorta and arch for frontal impact cases,
- substantially more work is needed to produce a locally validated finite element representation of the human mediastinal contents.

ACKNOWLEDGMENTS

The funding for this research has been provided [in part] by private parties, who have selected Dr. Kennerly Digges [and FHWA/NHTSA National Crash Analysis Center at The George Washington University] to be an independent solicitor of and funder for research in motor vehicle safety, and to be one of the peer reviewers for the research projects and reports. Neither of the private parties have determined the allocation of funds or had any influence on the content of this report. This research was supported in part also by the National Highway Traffic Safety Administration through the Southern Consortium for Impact Biomechanics of the University of Alabama at Birmingham.

REFERENCES

Bass, C.R., Darvish, K., Bush, B., Crandall, J.R., Srinivasan, S.C.M., Tribble, C., Fiser, S., Tourret, L., Evans, J.C., Patrie, J., and Wang, C. (2001). Material properties for modeling traumatic aortic rupture. Stapp Car Crash Journal, 45, 143-160.

Burkhart, H. M., Gomez, G. A., Jacobson, L. E., Pless, J. E., and Broadie, T. A. (2001). Fatal Blunt Aortic Injuries: A Review of 242 Autopsy Cases. J Trauma, 50, 113-115.

Crass, J. R., Cohen, A. M., Motta, A. O., Tomashefski, J. F. Jr, and Wiesen, E. J. (1990). A proposed new mechanism of traumatic aortic rupture: the osseous pinch. Radiology, 176(3), 645-649.

Iwamoto, M., Miki, K., Mohammad, M., Nayef, A., Yang, K. H., Begeman, P. C., and King, A. I. (2000). Development of a Finite Element Model of the Human Shoulder. 44th Stapp Car Crash Journal, 44, 281-297.

Katyal, D., Mclellan, B. A., Brenneman, F. D., Boulanger, B., Sharkey, P. W., and Waddell, J. P. (1997). Lateral impact motor vehicle collisions: Significant cause of blunt traumatic rupture of the thoracic aorta. Journal of Trauma, 42(5), 769-772.

Klotz, O., and Simpson, W. (1932). Spontaneous Rupture of the Aorta. American Journal of Medical Science, 184, 455-473.

Lee, J. B., and Yang, K. H. (2001). Development of a finite element model of the human abdomen. 45th Stapp Car Crash Journal, 45, 79-100.

Letterer, E. (1924). Beitrage zur entstehung der aortenruptur an typischer stele. Virch. Arch. Path. Anat, 253, 534-544.

Lundevall, J. (1964). The Mechanism of Traumatic Rupture of the Aorta. Acta Path. Microbiol. Scand, 62, 34-46.

Maddali, M., Shah, C. S., and Yang, K. H. (2005). Finite Element Modeling of Aortic Tissue Using High Speed Experimental Data. Proceedings of IMECE05, 2005 ASME International

Mechanical Engineering Congress, IMECE2005-82083.
Mattox, K. L. (1989). Fact and fiction about management of aortic transaction. Ann Thorac Surg, 48, 1--2.
McGwin, G., Metzger, J., Moran, S. G., and Rue, L. W. (2003). Occupant- and Collision-Related Risk Factors for Blunt Thoracic Aorta Injury. J. Trauma, 54, 655-662.
Mohan, D. (1976). Passive mechanical properties of human aortic tissue. PhD Dissertation, University of Michigan, Ann Arbor.
Sauaia, A., Moore, F. A., Moore, E. E., et al. (1995). Epidemiology of trauma deaths: a reassessment. J. Trauma, 38, 185-193.
Shah, C. S., Hardy, W. N., Mason, M. J., Yang, K. H., Van Ee, C. A., Morgan, R., and Digges, K. (2006). Dynamic Biaxial Tissue Properties of the Human Cadaver Aorta. 50th Stapp Car Crash Journal, 50, 217-246.
Shah, C. S., Lee, J. B., Hardy, W. N., and Yang, K. H. (2004). A Partially Validated Finite Element Whole-Body Human Model for Organ Level Injury Prediction. Proceedings of IMECE04, 2004 ASME International Mechanical Engineering Congress, IMECE2004-61844.
Shah, C. S., Maddali, M., Mungikar, S. A., Beillas, P., Hardy, W. N., Yang, K. H., Bedewi, P. G., Digges, K., and Augenstein, J. (2005a). Analysis of a Real-World Crash Using Finite Element Modeling to Examine Traumatic Rupture of the Aorta. Occupant Safety, Safety-Critical Systems, and Crashworthiness, SAE Paper No. 2005-01-1293.
Shah, C. S., Mason, M. J., Yang, K. H., Hardy, W. N., Van Ee, C. A., Morgan, R., and Digges, K. (2005b). High-Speed Biaxial Tissue Properties of The Human Cadaver Aorta. Proceedings of IMECE05, 2005 ASME International Mechanical Engineering Congress, IMECE2005-82085.
Shah, C. S., Yang, K. H., Hardy, W. N., Wang, K. H., and King, A. I. (2001). Development of a computer model to predict aortic rupture due to impact loading. 45th Stapp Car Crash Journal, 45, 161-182.
Steps, J. (2003). Crash Characteristics Indicative of Aortic Injury in Near Side Vehicle-to-Vehicle Crashes. Ph.D. Dissertation, The George Washington University.
Strassmann, G. (1947). Traumatic Rupture of the Aorta. American Heart Journal, 33, 508-515.
Voigt, G. E., and Wilfert, K. (1969). Mechanisms of injuries to unrestrained drivers in head-on collisions. Proc. 13th Stapp Car Crash Conference, pp. 295-313.
Zehnder, M. A. (1960). Accident Mechanism and Accident Mechanics of the Aortic Rupture in the closed Thorax Trauma. Thoraxchirurgie und Vasculaere Chirurgie, 8, 47-65.